

Corrosion Risk Prediction of Carbon Steels by Hyperspectral Analysis

Journal:	*ISIJ International*
Manuscript ID	ISIJINT-2026-046.R2
Manuscript Type:	Regular Article
Date Submitted by the Author:	n/a
Complete List of Authors:	Katayama, Hideki; National Institute for Materials Science, Research Center for Structural Materials Yoshida, Yuto; Hosei University Faculty of Bioscience and Chemistry Akashi, Takaya; Hosei University Faculty of Bioscience and Chemistry Kadowaki, Mariko; National Institute for Materials Science, Research Center for Structural Materials Murase, Yoshiharu; National Institute for Materials Science, Research Center for Structural Materials Tsutsumi, Yusuke; National Institute for Materials Science, Research Center for Structural Materials
If you choose "Instrumentation, Control and System Engineering", please select the most appropriate field.:	
Keywords (Please enter all keywords described to your manuscript.):	Hyperspectral measurement, Carbon steel, Corrosion, Corrosion product, Exposure test



Abstract:

The utility of hyperspectral measurement was assessed as a means of predicting the corrosion risk of steel materials based on surface information. Carbon steels exposed to outdoor conditions in Choshi and Miyakojima were used as the test specimens. Exposure tests were conducted every six months for a duration of two and a half years. Corrosion loss was calculated by comparing the weight of specimens before exposure tests and after removing corrosion products from the surface. Hyperspectral measurements were conducted on these specimens, with corrosion products identified through SAM (Spectral Angle Mapper) analysis. α-FeOOH, β-FeOOH, γ-FeOOH, and Fe_3O_4 were employed as reference data for SAM analysis. In both Choshi and Miyakojima test sites, γ-FeOOH was predominantly detected on the specimens after ordinary exposure tests, whereas Fe_3O_4 was prevalent on the specimens exposed to sheltered environments. The correlation between the proportion of each corrosion product identified through SAM analysis and the amount of corrosion change over one year was investigated. α-FeOOH showed a positive correlation with the amount of corrosion change, whereas the amount of corrosion change tended to decrease with an increase in the β-FeOOH fraction.

Keywords

Hyperspectral measurement; Carbon steel; Corrosion; Corrosion product; Exposure test.

For Peer Review

1. Introduction

A large portion of Japan's infrastructure was constructed during the period of rapid economic growth, and in recent years, corrosion-induced deterioration has emerged as a critical societal issue. Under current maintenance practices—where repair actions are taken only after significant structural damage has occurred—the cumulative cost required through 2048 is estimated to reach approximately 12.3 trillion yen. In contrast, preventive maintenance, which involves continuous monitoring and early-stage intervention before severe degradation develops, has been reported to reduce overall expenditures by nearly 50%[1]. However, local governments, which are responsible for managing approximately 90% of the nation's bridges, face persistent challenges including shortages of skilled maintenance personnel and high inspection costs. These constraints underscore the growing need for more efficient, convenient, and objective diagnostic technologies that can facilitate preventive maintenance.

Currently, corrosion assessment of social infrastructures relies predominantly on close-range visual inspection[2]. Such inspections are inherently subjective, as diagnostic outcomes heavily depend on the inspector's experience and judgment. To overcome these limitations, various optical diagnostic techniques have recently been proposed as objective and quantitative alternatives. For example, Choi et al.[3] developed a classification method in which corrosion images captured by digital cameras are characterized using color, texture, and shape, enabling automated discrimination of corrosion types such as uniform, crevice, pitting, fretting, and intergranular corrosion. Feliciano et al.[4] demonstrated that texture analysis of sequential surface images of ASTM A36 steel subjected to atmospheric corrosion testing can provide indicators of surface degradation rates. Hagiwara et al.[5] reported that homogeneity and spatial anisotropy in texture features extracted from surface images of steel sheet piles can be used to distinguish between non-corrosion, corrosion, and pitting corrosion conditions. While these methods enable the corrosion assessment based on the result of appearance, they primarily focus on identifying the presence, morphology, or extent of corrosion. For effective preventive maintenance management, however, it

For Peer Review

J-STAGE

is essential not only to quantitatively evaluate the current state of corrosion but also to predict corrosion risk—specifically, whether corrosion is likely to progress or remain stable under given conditions. Addressing this need requires diagnostic methods capable of detecting surface characteristics that are not readily captured through conventional imaging. Therefore, we focused on hyperspectral imaging, a technology that captures detailed spectral information across a wide wavelength range from the ultraviolet to the near-infrared regions.

Hyperspectral images provide detailed data that include both spatial distribution and spectral signatures associated with material properties[6]. This technology has recently been applied in diverse fields including degradation assessment of rubber sheets and concrete[7-9], and analysis of forest vegetation and vitality[10, 11]. Applications related to metal corrosion have also been reported[12], such as visualization of rust progression on vehicle frames. Moreover, Kobayashi et al. [13] used normalized index analysis of hyperspectral data to evaluate corrosion resistance of steel materials. However, normalized spectral indices primarily reflect the optical characteristics of surface rust, and their physical interpretations remain insufficiently understood.

In this study, we aim to develop a method for predicting corrosion risk of carbon steel based on surface information obtained through hyperspectral analysis. Corrosion products formed on outdoor-exposed carbon steel were identified using hyperspectral data, and the relationships between corrosion loss and the quantified corrosion products were examined. Through this investigation, we evaluate the potential of hyperspectral imaging as a predictive diagnostic tool for corrosion risk.

2. Experimental methods

2.1 Samples

Four known iron-based corrosion products—α-FeOOH, β-FeOOH, γ-FeOOH, and Fe_3O_4—were used as reference materials for obtaining spectra required for corrosion product identification. Prior to hyperspectral measurement, each sample was finely ground for approximately 10 minutes

J-STAGE

For Peer Review

using an agate mortar and pestle to ensure sufficient homogenization of the powder and to minimize surface irregularities.

Carbon steel specimens exposed to outdoor environments were used to evaluate the applicability of hyperspectral analysis to corrosion diagnosis. The chemical compositions of the steels are listed in Table 1. Each specimen had initial dimensions of 170 × 70 × 5 mm, and the surfaces were ground to a roughness of Ra 0.4–1.6 μm prior to exposure. Exposure tests were conducted at two locations operated by the Japan Weathering Test Center: the Choshi test site (35°43′N, 140°45′E) and the Miyakojima test site (24°44′N, 125°19′E). Both ordinary atmospheric exposure and sheltered exposure[14] tests were employed. The average environmental conditions recorded at each site during the exposure periods are summarized in Table 2. Specimens were exposed for five durations: 0.5, 1.0, 1.5, 2.0, and 2.5 years, with four specimens allocated to each period. Following exposure, corrosion loss was determined for three of the four specimens by chemically removing the corrosion products, measuring the cleaned specimen weight, and calculating the difference from the initial weight. The remaining specimen from each exposure group was reserved for hyperspectral imaging.

2.2 Hyperspectral measurements

Hyperspectral measurements were performed using a hyperspectral camera (NH-7, Eva Japan Co., Ltd.) capable of acquiring spectral images at a 5-nm resolution over a wavelength range of 350–1100 nm. An overview of the measurement system is shown in Fig. 1. During measurement, the sample was placed horizontally on a sample stage, and the hyperspectral camera was positioned vertically above the specimen. Three halogen lamps were used as illumination sources, arranged to irradiate the specimen simultaneously from three directions. To ensure uniform illumination, a light-diffusion box was installed around the specimen. Prior to specimen measurements, an image of a white reference board was captured to obtain light-source data. Subsequently, hyperspectral images of the samples were acquired. Reflectance spectra were calculated by dividing the spectral

For Peer Review

J-STAGE

radiance values at each pixel by the corresponding light-source data. Measurements were conducted either over the full area shown in Fig. 2 or within the rectangular region at the center of the specimen. For each sample, five hyperspectral images were collected, and the averaged spectrum was used for subsequent analysis. The imaging conditions were set to a scan rate of 100 lines/s and a gain of 50 throughout the measurements.

2.3 Hyperspectral analysis

Spectral Angle Mapper (SAM) analysis was used for the hyperspectral analysis. SAM analysis is widely used for hyperspectral data analysis[15, 16] because it allows for easy physical interpretation of results and has low computational load even for hyperspectral data with a large number of bands (number of measurable wavelengths). In SAM, substances are identified based on the spectral angle θ between a training vector s and a measured vector x, as illustrated in Fig. 3. The spectral similarity a between two spectra is defined in Equation (1). In this study, training vectors were constructed from hyperspectral data obtained for four types of iron-based corrosion products. Each training vector was defined using two selected wavelengths to ensure stable identification performance. These vectors were then compared with spectral vectors obtained from unknown corrosion products. The corrosion product type exhibiting the highest similarity value a was assigned as the identified iron rust.

$$a = \cos\theta = \frac{x \cdot s}{|x|\,|s|} \quad (1)$$

3. Results and Discussion

3.1 Hyperspectral measurements of known iron-based corrosion products

The hyperspectral measurement results for α-FeOOH, β-FeOOH, γ-FeOOH, and Fe_3O_4 are shown in Fig. 4. Distinct differences were observed among the spectra of the four corrosion products. α-FeOOH exhibited pronounced reflectance peaks near approximately 580 nm and 760

J-STAGE

For Peer Review

nm. β-FeOOH showed a characteristic reflectance peak around 740 nm, whereas γ-FeOOH displayed notable reflectance near approximately 600 nm and 790 nm. In contrast, Fe_3O_4, which is a black corrosion product, did not present any identifiable spectral features and exhibited low reflectance across the measured wavelength range. These findings demonstrate that hyperspectral imaging is capable of distinguishing among the four types of iron-based corrosion products based on their spectral characteristics.

3.2 Examination of analysis wavelengths in SAM analysis

As described in Section 2.3, SAM analysis utilizes two wavelengths, and therefore the selection of these wavelengths can influence identification accuracy. Pixel-by-pixel SAM analysis was conducted to determine the optimal wavelength combination, and the investigation was conducted based on the classification accuracy of corrosion products in the hyperspectral images. Pixel-based identification accuracy was evaluated using bitmap image editing software (GIMP: GNU Image Manipulation Program), which allows counting of pixel numbers corresponding to each mapped color. Based on the spectral characteristics shown in Fig. 4, one of the analysis wavelengths was fixed at 500 nm, where all three FeOOH species exhibit minimal reflectance. The other wavelength was investigated from 750 nm to 800 nm at 10 nm intervals, corresponding to the region where FeOOH shows distinct spectral features.

Figure 5 shows the identification accuracy for γ-FeOOH. Here, the identification accuracy was defined as the ratio of the number of pixels identified as the target corrosion product by SAM analysis to the total number of pixels. The circular parts in the figure represent the deposition areas of γ-FeOOH, and the colors were set in this study as follows: α-FeOOH (blue), β-FeOOH (yellow), γ-FeOOH (red), and Fe_3O_4(gray). Identification accuracies for the other corrosion products were evaluated across the same wavelength range, and the results are summarized in Table 3. The identification accuracy of γ-FeOOH exceeded 99% at all analysis wavelengths, although it was highest between 750 and 770 nm and decreased slightly at wavelengths of 780 nm and higher.

For Peer Review

Fe_3O_4 exhibited little variation in accuracy across wavelengths, whereas α-FeOOH and β-FeOOH showed improved identification performance at 750 nm and 760 nm.

Figure 6 illustrates the slopes of the spectral vectors for each corrosion product at 750 and 800 nm. The vector for β-FeOOH lies between those of α-FeOOH and γ-FeOOH, showing a tendency to shift closer to α-FeOOH at 800 nm and toward γ-FeOOH at 750 nm. Because SAM analysis provides better discrimination when the angular separation between vectors is larger, the wavelength pair that maximizes spectral angle differences yields the highest classification accuracy. Based on these considerations, 500 nm and 760 nm were selected as the wavelengths selected for SAM analysis of iron-based corrosion products in this study.

3.3 Results of outdoor exposure tests

Figure 7 shows the changes in corrosion loss over time for carbon steels after ordinary and sheltered exposure tests at the Choshi and Miyakojima Test Sites. In all environmental conditions, corrosion loss increased with exposure duration, with the increase being more pronounced at the Miyakojima test site, which represents a more severe corrosive environment. In this study, corrosion loss in ordinary exposure test was greater than that in sheltered exposure test at both test sites up to the first year. Although it is well known that the ordinary exposure test causes less severe corrosion than sheltered exposure test because adhered corrosive substances such as airborne sea salt are washed away by rainfall[17-19], the influence of wetting due to rainfall or dew condensation was considered to have played a dominant role in corrosion progression during the first year of exposure test in this study. In contrast, from 1.5 years onward, corrosion loss in sheltered exposure test exceeded that in ordinary exposure test. Under sheltered conditions in coastal environments, adhered airborne sea salt is not removed by rainfall, allowing it to accumulate on the steel surface. The deposited sea salt readily absorbs moisture from the atmosphere, resulting in exposure to concentrated salt solutions for long time and consequently accelerating corrosion. This effect became particularly evident between the 2.0- and 2.5-year

For Peer Review

exposure periods, during which the increase in corrosion loss in sheltered exposure test was substantially larger than that observed in ordinary exposure test.

3.4 Identification of corrosion products formed on exposed test specimens using SAM analysis

Hyperspectral measurements and SAM analyses were performed for all specimens subjected to ordinary and sheltered exposure tests at both the Choshi and Miyakojima Test Sites. As an example of two-dimensional mapping, the results for specimens after exposure tests for 1.5 years are presented in Fig. 8. At both test sites, γ-FeOOH was predominantly detected on the specimens subjected to ordinary exposure test, whereas Fe_3O_4 was primarily identified on those exposed under sheltered conditions.

The formation mechanisms of iron corrosion products generally can be interpreted using the Evans Model[20, 21]. According to this model, corrosion products generated under drying conditions in the daytime are predominantly FeOOH species through the following reactions:

$$Fe \rightarrow Fe^{2+} + 2e^{-} \quad (2)$$

$$2Fe^{2+} + \frac{1}{2}O_2 + 3H_2O \rightarrow 2FeOOH + 4H^{+} \quad (3)$$

$$Fe^{2+} + 8FeOOH + 2e^{-} \rightarrow 3Fe_3O_4 + 4H_2 \quad (4)$$

Under humid conditions, however, corrosion products undergo reduction, and dissolution of iron proceeds simultaneously. The generated Fe^{2+} can react with FeOOH to produce iron oxides with lower oxidation states, resulting in a higher proportion of Fe_3O_4. Thus, the formation of Fe_3O_4 is considered to dominate under prolonged humid conditions[22]. The corrosion-inducing substances such as airborne sea salt accumulate on specimen surfaces under the sheltered condition in coastal areas, where rainfall does not wash them away. This accumulation promotes extended periods of surface wetness due to the water absorption of sea salt. Therefore, the detection results of iron-based corrosion products shown in Fig. 8 can be considered reasonable.

For Peer Review

3.5 Relationship between surface presence ratio of corrosion products and corrosion change amount

It is essential to clarify the correlation between change in corrosion evaluation parameters and change in corrosion loss to predict future corrosion risk based on the surface characteristics of steel materials. Corrosion products formed on steel surfaces are not only a consequence of corrosion behavior but can also strongly influence subsequent corrosion performance. Yamashita et al. [23, 24] proposed evaluating the protective performance of rust layers formed on weathering steel using the mass ratio of α-FeOOH to γ-FeOOH (the α/γ value) obtained through internal-standard quantitative X-ray diffraction method. Rust layers were diagnosed as protective when this value exceeded 2. They later revised the index to the α/γ* value—defined as α-FeOOH divided by (γ-FeOOH + β-FeOOH + Fe_3O_4)—to apply for exfoliating rust formed in coastal areas[25].

Figure 9 shows the relationship between the surface presence ratio of each corrosion product obtained by SAM analysis and the change in corrosion loss for the subsequent one-year period. Although specimens were collected every 0.5 years, short-term corrosion loss may be greatly influenced by seasonal environmental fluctuations. Therefore, the change in corrosion loss for one-year was used for the analysis in this study. For example, the surface presence ratios of each corrosion product obtained from hyperspectral analysis of specimens exposed for 0.5 years were linked to the difference between the corrosion loss at 0.5 years and the corrosion loss at 1.5 years. No clear correlation with the change in corrosion loss was observed for γ-FeOOH and Fe_3O_4, indicating that neither corrosion product is suitable as a direct predictor of corrosion progression. However, as shown previously in Fig. 8, γ-FeOOH was predominantly detected in ordinary exposure test, whereas Fe_3O_4 was prevalent in sheltered exposure test. This result suggests that their presence ratios provide the information of environmental conditions—specifically wet condition.

A positive correlation with change in corrosion loss was observed for α-FeOOH. Generally, α-FeOOH is known as a thermodynamically stable corrosion product[25], and it is shown that the

J-STAGE

For Peer Review

estimation of protective properties of corrosion products by α/γ and α/γ* is useful for weathering steel. This means that as the proportion of α-FeOOH in the corrosion products increases, the protective properties of the corrosion products increase, suppressing corrosion. However, while the rust layer formed on weathering steel has a two-layer structure consisting of an outer and inner layer, it has been reported that FeOOH and Fe_3O_4 coexist in the case of carbon steel[26]. Therefore, the role of each corrosion product cannot be considered in the same way as that of weathering steel.

One possibility that α-FeOOH presence on the surface has a negative effect on corrosion resistance is that its microstructure may make them more susceptible to condensation and capillary condensation. Okada et al.[27] reported that the particle size of α-FeOOH formed under atmospheric environment was very small using Mössbauer spectroscopy. As shown in Eq. (5), it is known that the vapor pressure (P) on a liquid surface with a concave surface is smaller than the vapor pressure (P_0) on a normal liquid surface with no curvature. The smaller the curvature radius of a pore, the smaller the saturated vapor pressure, and water condensation occurs even if the humidity does not reach 100%.[28]

$$\log_{10}\frac{P}{P_0} = \frac{-2\sigma V}{r\mathrm{R}T} \quad (5)$$

where ρ is the surface tension, V is the molar volume, r is the capillary radius, R is the gas constant, and T is the absolute temperature. Therefore, α-FeOOH-rich surfaces may retain moisture more readily, increasing the wetness duration and accelerating corrosion.

In contrast, β-FeOOH showed a trend of decreasing corrosion loss as its surface presence ratio increased. β-FeOOH is generally recognized as a corrosion product generated under severe corrosion environments with a large amount of airborne sea salt[29] and it is suggested that there is a correlation between the corrosion loss and β-FeOOH presence. Although the present results indicate the opposite, this trend agrees with the findings of Shinohara et al. [30], who reported reduced corrosion loss in Fe–Ni alloys as β-FeOOH content increased. This inhibitory effect is

J-STAGE

For Peer Review

likely related to the chloride-binding capability of β-FeOOH. β-FeOOH is known to contain Cl^- between the network structure of $FeO_3(OH)_3$ octahedra that make up its crystals[31], effectively immobilizing Cl^-. This fixation of chloride ions[22] may have suppressed the penetration of Cl^- into the inner rust layer or substrate, thereby limiting corrosion propagation.

The SAM analysis of hyperspectral in this study successfully identified four types of corrosion products—α-FeOOH, β-FeOOH, γ-FeOOH, and Fe_3O_4—and demonstrated that the surface presence ratios of α-FeOOH and β-FeOOH correlate with the subsequent corrosion change. These results indicate the potential of hyperspectral surface analysis as a non-destructive tool for predicting corrosion risk. However, SAM analysis identifies phases based on spectral similarity. When similarity values fall below 1, the classification defaults to the closest reference spectrum, which may affect the accuracy when mixed corrosion products are present. The more training spectra data need to be collected using samples containing multiple kinds of corrosion products to improve identification accuracy.

4. Conclusion

In this study, hyperspectral analysis was examined as a diagnostic tool for predicting corrosion risk based on the surface characteristics of steel materials. Hyperspectral imaging was conducted on carbon steel specimens exposed to outdoor environments, the corrosion products formed were identified, and the relationship between the surface presence ratios of individual corrosion products and corrosion loss was investigated. The main findings are summarized as follows:

1) SAM analysis of hyperspectral data enables quantitative evaluation of the identification ratios of corrosion products formed on the surface of carbon steel.
2) γ-FeOOH was predominantly detected on specimens subjected to ordinary exposure tests, whereas Fe_3O_4 was mainly detected on specimens exposed under sheltered conditions.
3) With respect to the one-year change in corrosion loss, the surface presence ratio of α-FeOOH showed a positive correlation, while that of β-FeOOH showed a negative

For Peer Review

correlation.

4) The usefulness of hyperspectral surface appearance measurements as a technique for predicting corrosion risk in carbon steel was confirmed.

Statement for Conflict of Interest

The authors have no conflicts of interest directly relevant to the content of this article.

Acknowledgments

This study was conducted with the support of the Japan Iron and Steel Institute Research Committee I "Data Science Research Committee for Infrastructure Deterioration Diagnosis." We express our sincere gratitude.

References

1) Ministry of Land, Infrastructure, Transport and Tourism, Government of Japan: Document of Cabinet Office, (Promotion for preventive maintenance countermeasures of ageing infrastructures), (November 5, 2020), https://www5.cao.go.jp/Keizai-shimon/kaigi/special/reform/wg6/20201110/pdf/shiryou1-1.pdf, (accessed 2024-04-19) (in Japanese).

2) Ministry of Land, Infrastructure, Transport and Tourism, Government of Japan: Document of Cabinet Office, (Guidelines for periodic inspection of road bridges), (February, 2019), https://www.mlit.go.jp/road/sisaku/yobohozen/tenken/yobo4_1.pdf, (accessed 2024-04-19) (in Japanese).

3) K. Y. Choi and S. S. Kim: *Corrosion Science*, 47(2005), 1. https://doi.org/10.1016/j.corsci.2004.05.007

4) F. F. Feliciano, F. R. Leta, and F. B. Mainier: *Corros. Sci.*, 93(2015), 138. http://dx.doi.org/10.1016/j.corsci.2015.01.017

For Peer Review

5) T. Hagiwara, Y. Shimamoto, T. Suzuki, N. Otaka, and Y. Fujimoto: *IDRE Journal*, 88(2020), 145 (in Japanese). https://doi.org/10.11408/jsidre.88.I_145

6) S. Ono: *IEICE ESS Fundamentals Review*, 14(2020), 138 (in Japanese). https://doi.org/10.1587/essfr.14.2_138

7) J. Arita, T. Endo, K. Okuyama, S. Ochi, and Y. Yasuoka: *SEISAN KENKYU*, 53(2001), 615 (in Japanese). https://doi.org/10.11188/seisankenkyu.53.615

8) T. Nakajima, T. Endo, and Y. Yasuoka: *SEISAN KENKYU*, 56(2004), 190 (in Japanese). https://doi.org/10.11188/seisankenkyu.56.190

9) D. B. Siano, W. Abdullakasim, A. Terdwongworakul, and K. Phuangsombut: *Sens. Bio-Sens. Res.*, 33(2021), 1. https://doi.org/10.1016/j.sbsr.2021.100441

10) H. P. Sato, S. Miyasaka, H. Makita, H. Yagi, M. Korai: *J. of JSPRS*, 45(2006), 32 (in Japanese). https://doi.org/10.4287/jsprs.45.5_32

11) Y. Morikawa and I. Furukawa: *Research Bulletin of Tottori University Forestry*, 24(1996), 55 (in Japanese).

12) Iris Co.: Report for Quality management, https://hokkaido-sat.co.jp/quality_management, (accessed December 22, 2023) (in Japanese).

13) Ryo Kobayashi, Hideki Katayama, Takaya Akashi: *Materials and Environment*, 70(2021), 354 (in Japanese). https://doi.org/10.3323/jcorr.70.354

14) JIS Z 2381: 2017, General requirements for atmospheric exposure testing (in Japanese).

15) Yasushi YAMAGUCHI: *Journal of the Remote Sensing Society of Japan*, 39(2019), 241 (in Japanese). https://doi.org/10.11440/rssj.39.241

16) Y. Amano and N. Takagi: *J. Environ. Eng.*, 70(2005),49 (in Japanese). https://doi.org/10.3130/aije.70.49_1

17) T. Shinohara: *Journal of the Society of Surface Science and Technology of Japan*, 36(2015), 4 (in Japanese). https://doi.org/10.1380/jsssj.36.4

18) S. Hara, M. Miura, Y. Utsumi, T. Fujiwara, and M. Yamamoto: *Materials and Environment*,

For Peer Review

331 54(2005), 344 (in Japanese). https://doi.org/10.3323/jcorr1991.54.344
332 19) M. Takeba, M. Ohya, R. Adachi, S. Ajiki, J. Ota, R. Gan-ei, N. Kiatagawa, T. Furukawa, Y.
333 Matsuzaki, and T. Aso: *Materials and Environment*, 57(2008), 188 (in Japanese).
334 https://doi.org/10.3323/jcorr.57.188
335 20) U. R. Evans: *Corrosion Science*, 9(1969), 813. https://doi.org/10.1016/S0010-
336 938X(69)80074-0
337 21) U. R. Evans and A. A. J. Taylor: *Corrosion Science*, 12(1972), 227.
338 https://doi.org/10.1016/S0010-938X(72)90671-3
339 22) T. Ohtsuka: 211th and 212th Nishiyama Memorial Seminar, ISIJ, Tokyo, (2012), 8 (in
340 Japanese).
341 23) M. Yamashita, H. Miyuki, H. Nagano, and T. Misawa: *Materials and Environment*, 43(1994),
342 26 (in Japanese). https://doi.org/10.3323/jcorr1991.43.26
343 24) M. Yamashita, H. Miyuki, and H. Nagano: *Sumitomo Met.*, 47(1995), 4 (in Japanese).
344 25) T. Kamimura, M. Yamashita, H. Uchida, H. Miyuki: *Journal of the Japan Institute of Metals*
345 *and Materials*, 65(2001), 922 (in Japanese). https://doi.org/10.2320/jinstmet1952.65.10_922
346 26) H. Okada, Y. Hosoi, K. Yukawa, H. Naito: *Iron and Steel*, 55(1969), 355 (in Japanese).
347 https://doi.org/10.2355/tetsutohagane1955.55.5_355
348 27) T. Okada, Y. Ishii, T. Mizoguchi, I. Tamura, Y. Kobayashi, Y. Takagi, S. Suzuki, H. Kihira,
349 M. Itou, A. Usami, K. Tanabe, and K. Masuda: *Jpn. J. Appl. Phys.*, 39(2000), 3382.
350 https://doi.org/10.1143/JJAP.39.3382
351 28) I. Matsushima: *Journal of the Japanese Society for Color and Materials*, 49(1976), 669 (in
352 Japanese). https://doi.org/10.4011/shikizai1937.49.669
353 29) T. Misawa: *CORROSION ENGINEERING*, 32(1983), 657 (in Japanese).
354 https://doi.org/10.3323/jcorr1974.32.11_657
355 30) National Institute for Materials Science: NIMS Materials Data Sheet Technical Document
356 No.18, NIMS, Tsukuba, (2006), 55 (in Japanese).

For Peer Review

357 31) U. Schwertmann and R. M. Cornell: Iron Oxides in the Laboratory, Wiley-VCH, Weinheim,
358 (2000), 1.
359
360

For Peer Review

361

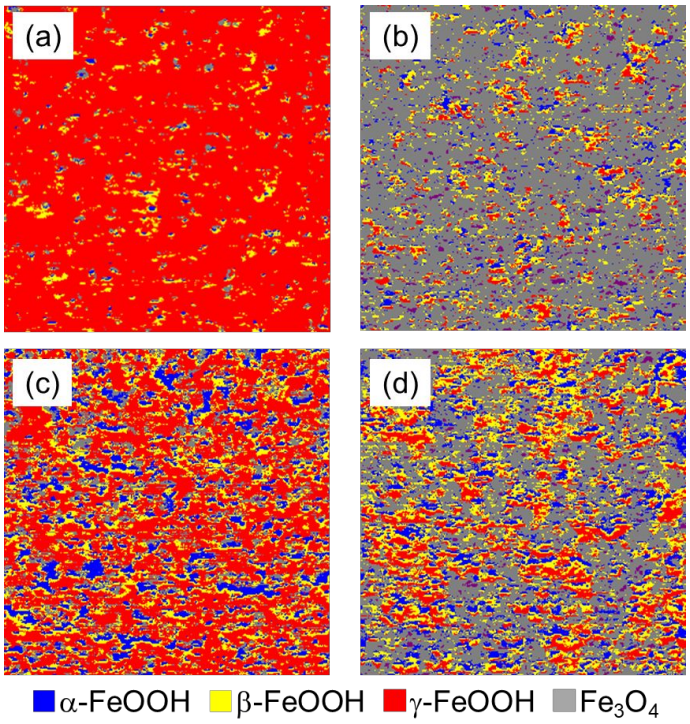

Graphical Abstract

362

view

Table 1 Chemical compositions (mass%) of specimens.

C	Si	Mn	P	S	Fe
0.17	0.02	1.07	0.013	0.003	Balance

(mass%)

For Peer Review

Table 2 Average values of environmental data during exposure tests at Choshi and Miyakojima test sites.

	Choshi	Miyakojima
Ave. Air Temp. (℃)	16.8	24.4
Ave. RH (%)	78.4	83.3
Monthly Precipitation (mm)	162.1	178.7
Chloride deposition Rate (mg NaCl/(m²·d))	15.8	34.1

For Peer Review

Table 3 Identification fraction of corrosion products by SAM analysis using each wavelength.

	750	760	770	780	790	800
α-FeOOH	94.3	93.3	92.6	92.4	92.2	92.0
β-FeOOH	99.9	99.9	99.9	99.6	98.5	97.4
γ-FeOOH	99.9	99.9	99.9	99.6	99.2	99.2
Fe_3O_4	99.9	99.9	99.9	99.9	99.9	99.9

(%)

For Peer Review

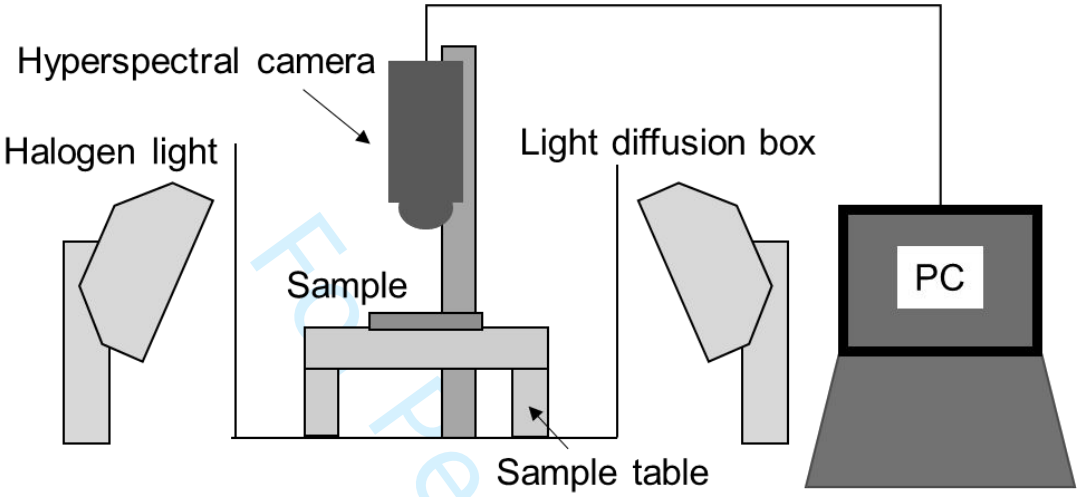

Fig. 1 Scheme of the hyperspectral measurement system.

For Peer Review

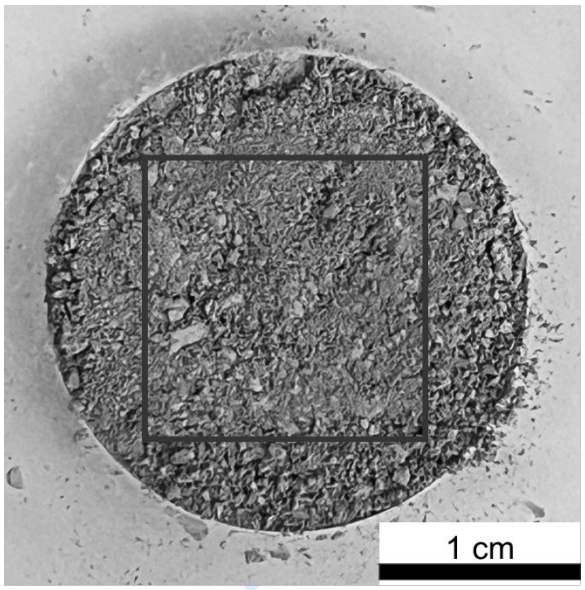

Fig. 2 Hyperspectral measurement area.

For Review

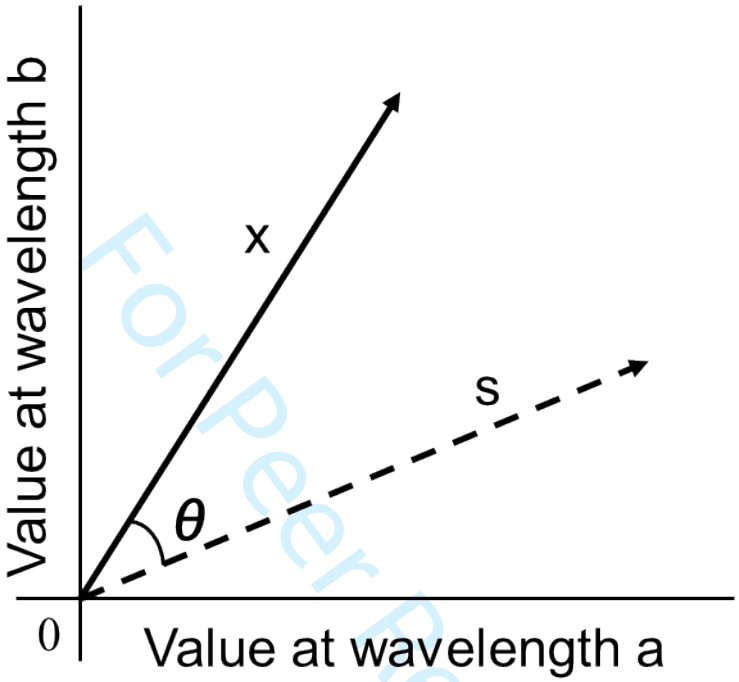

Fig. 3 Conceptual diagram of SAM.

For Peer Review

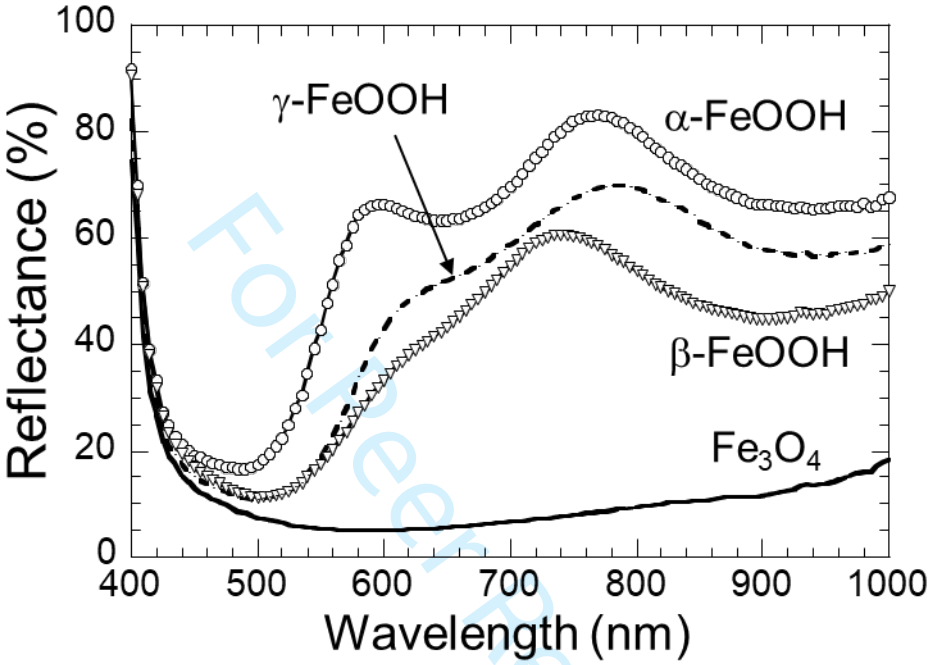

Fig. 4 Reflection spectra of α-FeOOH, β-FeOOH, γ-FeOOH and Fe_3O_4 using hyperspectral camera.

For Peer Review

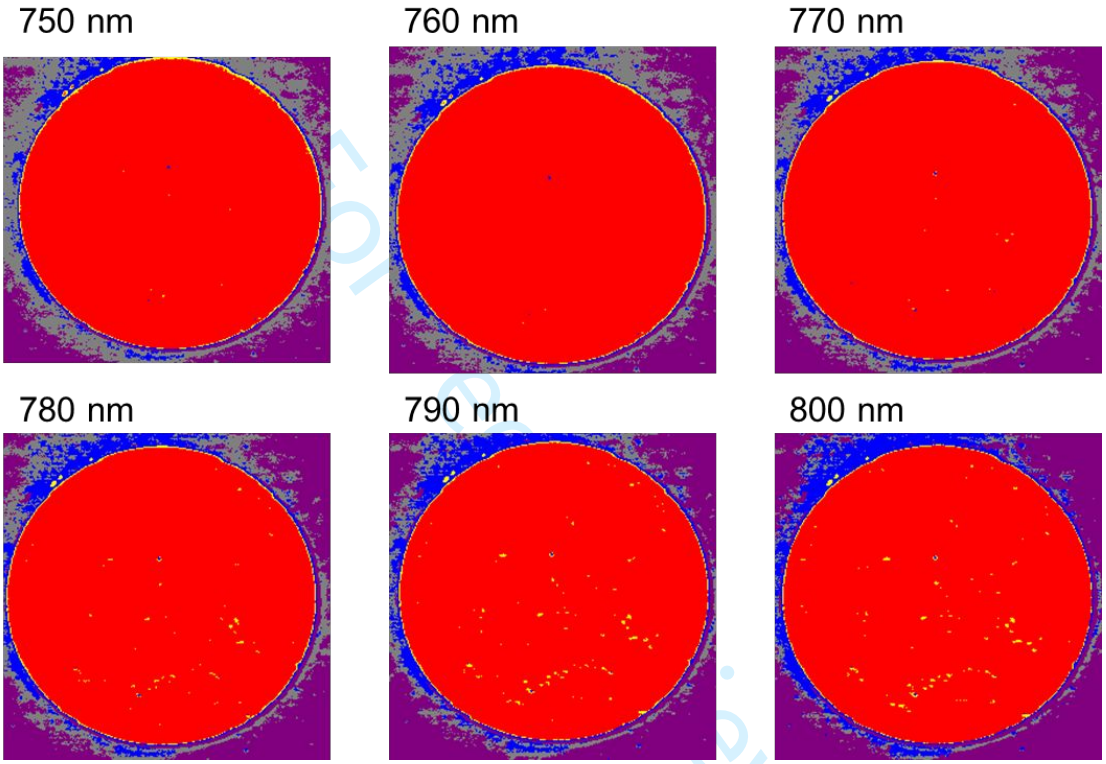

Fig.5 Identification fraction of γ-FeOOH by SAM analysis using each wavelength; α-FeOOH; blue, β-FeOOH; yellow, γ-FeOOH; red, Fe_3O_4; gray. **(color in print)**

J-STAGE

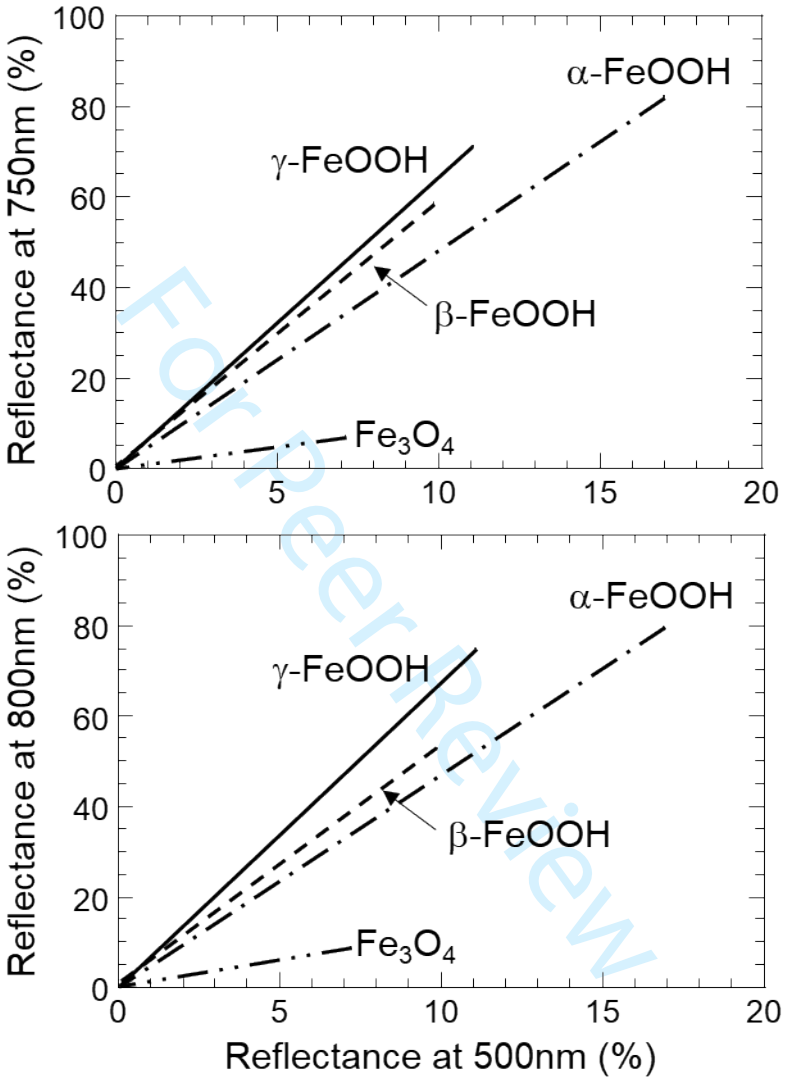

Fig. 6 SAM classification for each iron corrosion product.

For Peer Review

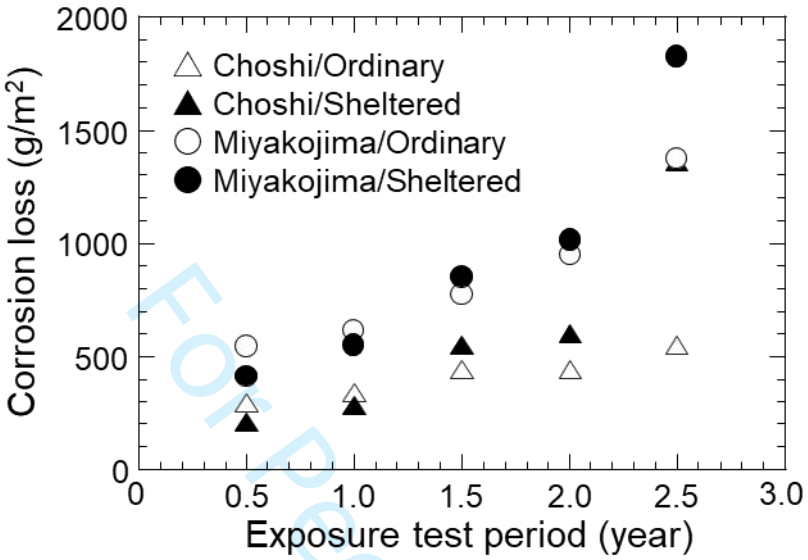

Fig.7 Change over time of corrosion loss of carbon steels exposed to ordinary and sheltered environments at Choshi and Miyakojima test sites.

For Peer Review

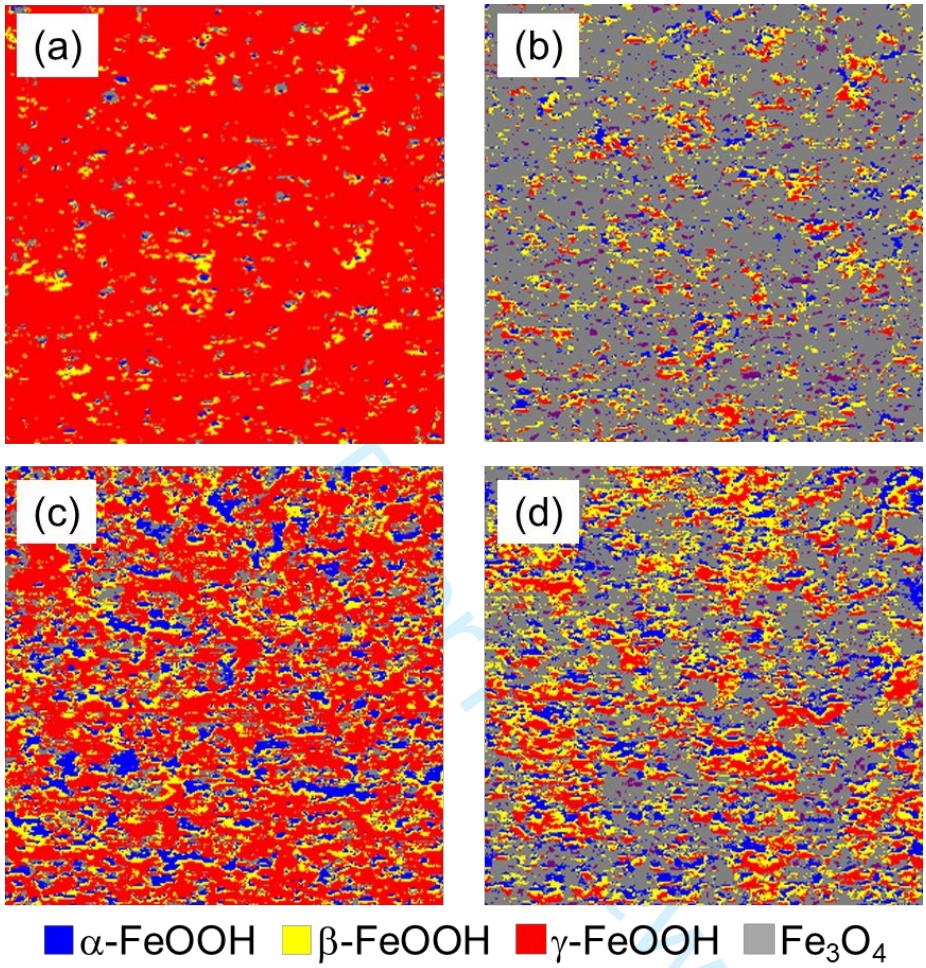

Fig.8 Two-dimensional mapping by SAM analysis for specimens exposed to outdoor environment for 1.5 years. (a) Ordinary exposure test at Choshi, (b) sheltered exposure test at Choshi, (c) ordinary exposure test at Miyakojima and (d) sheltered exposure test at Miyakojima. **(color in print)**

J-STAGE

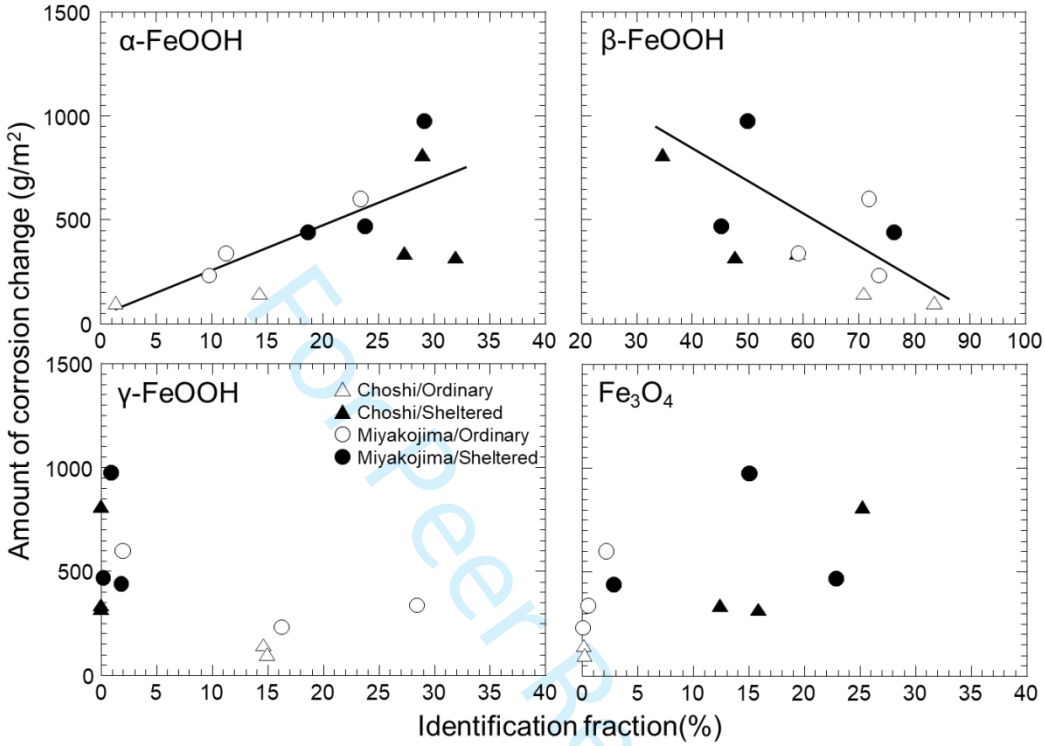

Fig.9 Relationship between the identification fraction of each corrosion product by SAM analysis and the change of corrosion loss over a year.

For Peer Review